The Effect of Pattern and Infill Percentage in 3D Printer for Phantom Radiation Applications

Aditya Prayugo Hariyanto, Kurnia Hastu Christianti, Agus Rubiyanto, Nasori, Mohammad Haekal, Endarko[*)]
Laboratory of Medical Physics and Biophysics, Department of Physics,
Institut Teknologi Sepuluh Nopember Surabaya
[*]E-mail: endarko@physics.its.ac.id

ABSTRACT

3D printing technology was capable of fabricating phantoms to enhance quality assurance in radiation therapy. The ideal phantom has properties equivalent to the real tissue. However, 3D Printing has the limits to mimicking the attenuation properties of various tissues because during 3D printing there can be only one type of material. The purpose of this study was to evaluate the effect of infill percentage and infill patterns of 3D printing technology to simulate various types of tissue. This study used 25 samples measuring $5 \times 5 \times 1$ cm^3 from PETG material. The 20 samples were printed using variations infill percentages from 5 - 100% and the infill pattern in lines. The five samples were then printed with the infill percentage constant at 50% and used the infill pattern triangles, grid, gyroid, octet, and concentric. We used Computed Tomography (CT) to determine the Hounsfield Unit (HU) value for each sample and evaluated the suitability of each sample for phantom applications in radiation therapy and radiology. However, none of the samples was able to simulate compact bone. As a result, we found that PETG material could simulate the properties of soft tissue, fat, lung, kidney, liver, pancreas, and spongy bone. Thus, the study had shown promising potential for the fabrication of the anthropomorphic phantom of radiation therapy.

Keywords: 3D printing, Hounsfield Unit (HU), PETG, Infill Percentage, Infill Pattern.

INTRODUCTION

3D printing technologies have benefited so extensively, especially in the health field. In radiation oncology. 3D printing technology produces bolus for radiotherapy patients in severe curvature areas, like the nose, feet, hands, and ears. As a result, tumor cells close to the skin can receive a maximum radiation dose while reducing the radiation dose to the organs at risk around them (Park *et al*., 2019). Furthermore, it is possible to create an anthropomorphic phantom with 3D printing technology to create patient-specific anatomy using Digital Imaging and Communications in Medicine (DICOM) Computed Tomography data (Okkalidis, 2018). The phantom is a real mimicking model with properties equivalent to the tissue (White, 1993). In radiodiagnostics, phantoms are important for assessing image quality, optimizing more realistic and controlled imaging systems (Mayer *et al*., 2015), and developing imaging techniques (Martini *et al*., 2020). Whereas in radiotherapy, specific anthropomorphic phantoms can improve the accuracy of quality assurance and control in radiation therapy treatment. However, the 3D printing technology has limited applications in quality assurance because 3D printing cannot bring about a variety of human body densities. 3D printing is used only in the type of material for the printing process (Oh *et al*., 2017).

When materials interact with X-ray radiation, the effects of radiation vary greatly depending on the density of each material (Choi *et al*., 2019; Kadoya *et al*., 2019). Therefore, quality assurance using uniform density phantoms would not be accurate or may even degrade the quality assurance of radiation treatment. Alternatively, it is possible to simulate the electron density of human tissue using the deposition method 3D printing technology by varying the infill density percentage of several filler patterns provided (Madamesila *et al*., 2016) by Ultimaker Cura software. The term fill pattern refers to the object's 3D internal structure, which can be either full or less densely filled depending on the given solid's fill setting. The maximum filling density, of course, is 100%; when the infill percentage decreases, the object becomes light, and there would be air gaps (Kairn *et al*., 2015; Okkalidis, 2018). Several studies related to the 3D printing infill setting have been carried out by Madamesila *et al*. indicate that the infill parameters used the High Impact Polystyrene (HIPS) material provide densities from 0.4 to 0.75. In addition, the result of the study of materials for low- dan high-density lung

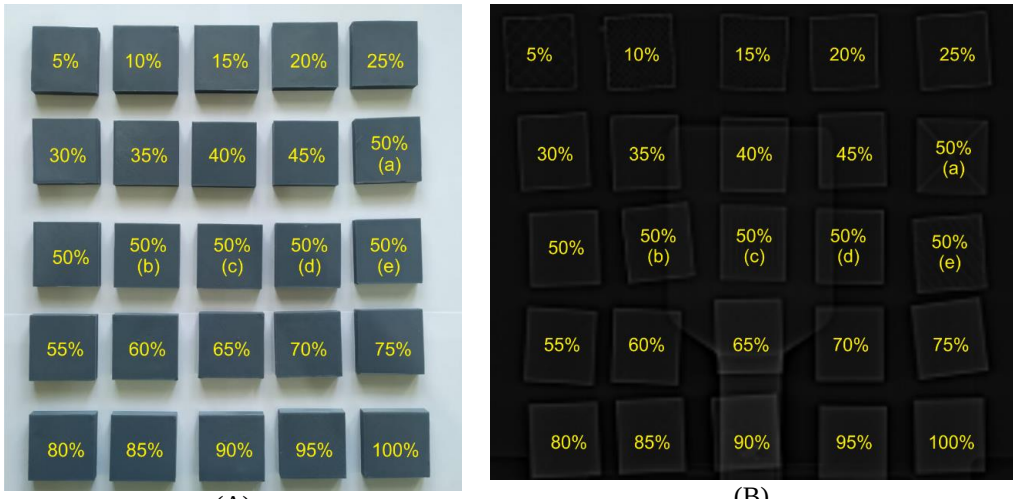

(A) (B)

Figure 1. (A) Photographic image of samples from 5 – 100% infill, a) Concentric, b) Grid, c) Gyroid, d) Octet, e) Triangles. (B) Tpogram image of the samples from 5 - 100% infill,) Concentric, b) Grid, c) Gyroid, d) Octet, e) Triangles obtained from CT-Scan.

replacements that were 3D printed had -794 ± 120 HU and -487 ± 35 HU, respectively (Madamesila *et al*., 2016). Furthermore, Kairn *et al*. have also taken a similar approach to Madamesila J. *et al*. using Acrylonitrile Butadiene Styrene (ABS) materials. The result showed that an infill of 30% for ABS had potential like lung phantoms and infill 90% correlated with tumor, muscle, and other soft tissue density. Therefore, this study will evaluate the density of Polyethylene Terephthalate (PETG) material using various patterns and infill percentages for radiation phantom applications. The choice of PETG material as a phantom radiation material was because this material was easily obtained commercially, had a density of 1.23 g/cm^3, and was easier to set up than ABS material. The evaluation process involved evaluating geometric (mass) printing accuracy and tissue equivalence through the Hounsfield Unit (HU) value so that 3D printing techniques can be widely adopted for anthropomorphic phantoms in the future.

METHODS

We used PETG filament from Shenzhen eSun Industrial CO., Ltd. with the best print and bed temperature characteristics, 230-250°C and 60-80°C, respectively. We made 25 samples of PETG material in the form of a box measuring 5×5×1 cm^3. Sample fabrication used 3D Creality CR 10 MAX (Shenzhen Creality 3D Technology CO. Ltd. China) with a general printing setting shown in Tabel 1. Printing of 20 samples was carried out by varying percentage infill from 5-100% with increment of 5%, lines pattern. Furthermore, the remaining five samples were printed with variations in inner structure patterns (Grid, Concentric, Gyroid, Octet, and Triangles), the infill percentage kept constant at 50%. All samples were measured for mass using Vernier Analytical Balance Type VAB2104. Then, the percentage difference between the sample printing mass and the estimated mass (obtained from Ultimaker Cura 4.7) can be calculated using equation (1).

$$\%\, diff = \left|\frac{m_a - m_e}{m_e}\right| \times 100\% \qquad (1)$$

where $m_a$is the printing mass (g) and m_e is the estimated mass (g).

Table 1. General setting for 3D printing Fused Deposition Method (FDM)

Arrangement	Value
Layer Height	0.2 mm
Initial Layer Height	0.2 mm
Wall Thickness	0.8 mm
Infill Density	5 - 100%
Infill Pattern	Lines
Printing Temperature	235 ℃ (PETG)
Build plate Temperature	60 ℃ (PETG)

A total of 25 samples were scanned using a CT Scanner under a set of 120 kV, 480 mA, 1 mm thickness. Figure 1. Shown the results of photographic images and topogram images from 25 PETG samples.

Hounsfield Unit (HU) is the value that contains the grey level of the CT image and can be calculated through the linear attenuation coefficient value as follows (Khan & Gibbons (Jr.), 2014):

Table 2. Percentage of difference in printing mass to the estimated mass by Ultimaker Cura

Infill Density (%)	Printing Mass (g)	Estimated Mass (g)	Difference (%)
5	5.709	5.7	0.158
10	7.071	7.1	0.408
15	8.471	8.4	0.845
20	9.839	9.8	0.398
25	11.292	11.1	1.730
30	12.621	12.5	0.968
35	14.101	13.8	2.181
40	15.831	15.2	4.151
45	17.172	16.8	2.214
50	17.765	17.9	0.754
55	19.815	19.2	3.203
60	21.538	20.6	4.553
65	22.747	21.9	3.868
70	24.071	23.3	3.309
75	25.211	24.6	2.484
80	26.341	26	1.312
85	27.101	27.3	0.729
90	28.535	28.7	0.575
95	29.709	29.8	0.305
100	30.132	31.1	3.113
50 (triangular)	17.698	17.9	1.128
50 (octec)	17.77	17.9	0.726
50 (gyround)	17.852	17.6	1.432
50 (Concentric)	17.519	17.5	0.109
50 (grid)	17.861	17.9	0.218

$$HU = \frac{\mu_{material} - \mu_{water}}{\mu_{water}} \times 1000 \qquad (2)$$

where $\mu_{material}$ is the linear attenuation coefficient for specific materials and μ_{water} is the linear attenuation coefficient of water. Air has a HU value equal to -1000 because the linear attenuation coefficient of air is 0, and water has a HU value equal to 0. In this study, we created a region of interest (ROI) derived from the appearance of the axial CT image to evaluate the HU value for each sample. The average value of HU obtained from PETG material with an infill percentage of 5-100% was presented in a graph where the x-axis was the infill percentage, and the y-axis was the average value of HU. Furthermore, the graph was analyzed by the fitting method using the linear equation below:

$$HU = a.infill\ density + b \qquad (3)$$

Moreover, the mean value of HU was also obtained from PETG with variations in the internal structure filling pattern shown in Table 4 for us to compare.

RESULTS AND DISCUSSION

As shown in Table 2, the percentage difference between the printing mass and the estimated was calculated using equation (1). Generally, the printing mass of PETG material had a slightly larger value than the estimated Ultimaker Cura. The percentage difference between the printing mass over the estimated mass was between <5%, and the variation in printing mass was still within the acceptable range. The average value of HU overall was obtained at 1.635%.

Table 3. Fitting parameter values and R-squared values for curves of PETG material

Material	Parameter		R-squared
	a	b	
PETG	-1016.23	11.45	0.999

PETG: Polyethylene Terephthalate shows the correlation of the average HU value to the infill value of the Polyethylene Terephthalate (PETG) material. The average HU value of Polyethylene Terephthalate (PETG) material from 5 - 100% infill variation was -961.17 ± 42.97 to 140.3 ± 10.22.

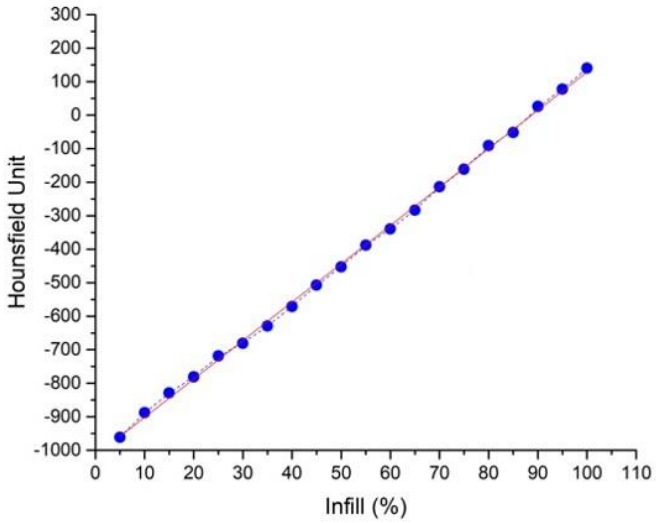

Figure 2. The correlation between the Hounsfield Unit (HU) value and the percentage infill value of Polyethylene Terephthalate (PETG) material were plotted with a blue dash line. The linear fitting curve for PETG was plotted with a solid line in red

Table 4. Effect of 3D printing infill pattern on HU value

Infill (%)	Pattern	HU Value			SD
		Mean	Min	Max	
50	Lines	-452.45	-435	-464	7.94
	Triangles	-463.17	-571	-310	84.20
	Octet	-451.14	-843	-210	187.14
	Gyroid	-425.27	-440	-415	6.48
	Concentric	-460.57	-466	-455	3.03
	Grid	-443.38	-485	-404	25.80

SD: Standard of Deviation, Min: Minimum, Max: Maximum

Table 5. The typical value of the Hounsfield Unit (HU) for human tissue (Kalender, 2011)

Tissues	HU Range
Air	-1005 to -995
Lung	-950 to -550
Fat	-100 to -80
Water	-4 to 4
Kidney	20 to 40
Pancreas	30 to 50
Blood	50 to 60
Liver	50 to 70
Muscle, Soft Tissue	20 to 100
Adipose Tissue	-200 to -20
Spongious Bone	50 to 300
Compact Bone (Cortical)	>300

Next, for the fitting curve, followed equation (3). The result of fitting using a linear equation for PETG material was shown in Table 3. fitting with the linear equation had been successful. This result was following the study conducted by Yea *et al*., who obtained an R-squared linear fitting of 0.99 for the PLA (Oh *et al*., 2017), also obtained an R-squared linear fitting of 0.99 for PLA and 0.97 for HIPS materials (Park *et al*., 2019). Furthermore, the effect of the pattern on the HU values is shown in Table 4.

Based on the research of (Madamesila *et al*., 2016) the effect of the filling pattern could affect the size of the air gap and the value of HU. The size air of air gap and HU value played an important role in achieving equivalent tissue and image quality. Table 4 showed the effect of filling patterns on the HU values of the samples using line, triangle, octet, gyroid, concentric, and grid filling patterns because these patterns were available in the Ultimaker Cura 4 software. The calculation of the average HU value showed a relatively small difference, except for the gyroid infill pattern. It indicated that the gyroid infill pattern's air gap was larger than other infill patterns.

The HU value obtained and associated with the tissue HU value summarized by Kalender, 2011 is shown in Table 5. Based on Table 5, we had succeeded in simulating lung tissue using PETG material with an infill percentage of 10 - 45% (Kalender, 2011) and a high-density lung using a 50 - 55% and also infill pattern of lines, triangles, octet, gyroid, concentric, grid with constant infill at 50% (Kairn *et al.*, 2015). The PETG material with an infill percentage of 75 - 85% could represent adipose tissue. PETG material with an infill percentage of 90 - 95% could represent soft tissue, liver, blood, kidneys, and pancreas. Meanwhile, PETG with infill 100% represented spongy bone with a HU value of 140.3 ± 10.22 (Kalender, 2011). Furthermore, we evaluated the potential of PETG material to be used as a reference as a material to simulate the thorax body parts for quality assurance and control in radiotherapy. Based on Craft and Howell's research, to simulate the heart, breast, and lungs, can use PETG material with the percentage of line pattern filling, 95 - 100%, 80 - 85%, and 15 - 30%, respectively (Craft & Howell, 2017). In addition, to make lung tumor tissue mimicking, PETG material can be used with a line pattern filling percentage of 80-90% (Hazelaar *et al*., 2018).

Our study's PETG material successfully simulated soft and low-density tissues based on the analysis. However, they could not represent the high-density tissue such as compact bone. It was a challenge for the researcher to cover the limitations of high-density 3D printing technology. On the other hand, our study had successfully confirmed the feasibility of 3D printing the PETG material as a radiation phantom material that could represent soft tissue, adipose, lung, and spongy bone by varying the infill density and infill pattern. Moreover, there was a need to develop methods or materials for simulating high-density tissue like conducting combined 3D printing and casting methods or developing high-density 3D printing materials. Thus, the heterogeneous anthropomorphic phantoms can be achieved excellent, thereby improving the quality assurance process in radiation therapy.

CONCLUSION

The value of PETG material had successfully represented soft tissue and low-density organs by varying the infill percentage and infill pattern on 3D printed. The result indicated that 3D printing technology could help improve quality assurance in radiation therapy by producing a specific anthropomorphic phantom. On the other hand, we still need to develop methods or materials to represent high-density tissues.

ACKNOWLEDGEMENTS

This work was supported by the Institut Teknologi Sepuluh Nopember (ITS), RISTEK-BRIN under Penelitian Dasar Unggulan Perguruan Tinggi (PDUPT) (No. 966/PKS/ITS/2021).

REFERENCES

Choi CH, Kim JI & Park JM. 2019. A 3D-Printed Patient-Specific Applicator Guide For Use in High-Dose-Rate Interstitial Brachytherapy For Tongue Cancer: A Phantom Study. *Physics in Medicine & Biology*. **64**: 135002.

Craft DF & Howell RM. 2017. Preparation and Fabrication of A Full-Scale, Sagittal-Sliced, 3D-Printed, Patient-Specific Radiotherapy Phantom. *Journal of Applied Clinical Medical Physics*. **18**: 285-292.

Hazelaar C, van Eijnatten M, Dahele M, Wolff J, Forouzanfar T, Slotman B & Verbakel WFAR. 2018. Using 3D Printing Techniques to Create An Anthropomorphic Thorax Phantom For Medical Imaging Purposes. *Medical Physics*. **45**: 92-100.

Kadoya N, Abe K, Nemoto H, Sato K, Ieko Y, Ito K, Dobashi S, Takeda K & Jingu K. 2019. Evaluation of a 3D-Printed Heterogeneous Anthropomorphic Head and Neck Phantom For Patient-Specific Quality Assurance in Intensity-Modulated Radiation Therapy. *Radiological Physics and Technology*. **12**: 351-356.

Kairn T, Crowe SB & Markwell T. 2015. Use of 3D Printed Materials as Tissue-Equivalent Phantoms, in: Jaffray, D.A. (Ed.), World Congress on Medical Physics and Biomedical Engineering, June 7-12, 2015, Toronto, Canada, *IFMBE Proceedings*. *Springer International Publishing, Cham*, pp. 728-731.

Kalender WA. 2011. *Computed Tomography: Fundamentals, System Technology, Image Quality, Applications*. John Wiley & Sons.

Khan FM, Gibbons (Jr.) JP. 2014. *Khan's The Physics of Radiation Therapy*. Lippincott Williams & Wilkins.

Madamesila J, McGeachy P, Villarreal Barajas, JE & Khan R. 2016. Characterizing 3D printing in The Fabrication of Variable Density Phantoms For Quality Assurance of Radiotherapy. *Physica Medica AIFB.* **32**: 242-247.

Martini N, Koukou V, Michail C & Fountos G. 2020. Dual Energy X-ray Methods for the Characterization, Quantification and Imaging of Calcification Minerals and Masses in Breast. *Crystals*. **10**: 198.

Mayer R, Liacouras P, Thomas A, Kang M, Lin, L & Simone CB. 2015. 3D Printer Generated Thorax Phantom with Mobile Tumor for Radiation Dosimetry. *Review of Scientific Instruments*. **86**: 074301.

Oh SA, Kim MJ, Kang JS, Hwang HS, Kim YJ, Kim SH, Park JW, Yea JW & Kim SK. 2017. Feasibility of Fabricating Variable Density Phantoms Using 3D Printing for Quality Assurance (QA) in Radiotherapy. *Progress in Medical Physics*. **28**: 106.

Okkalidis N. 2018. A novel 3D Printing Method for Accurate Anatomy Replication in Patient-Specific Phantoms. *Medical Physics*. **45**: 4600-4606.

Park SY, Choi N, Choi BG, Lee DM & Jang N. 2019. Radiological Characteristics of Materials Used in 3-Dimensional Printing with Various Infill Densities. *Progress in Medical Physics*. **30**(4): 155.

Park SY, Kang S, Park JM, An HJ, Oh DH & Kim JI, 2019. Development and Dosimetric Assessment of A Patient-Specific Elastic Skin Applicator for High-Dose-Rate Brachytherapy. *Brachytherapy*. 18: 224-232.

White DR. 1993. The Design and Manufacture of Anthropomorphic Phantoms. *Radiation Protection Dosimetry*. **49:** 359-369.